

Bidirectional flow of two-dimensional dusty plasma under asymmetric periodic substrates driven by unbiased external excitations

Wei Li^{1,2 *}, D. Huang², C. Reichhardt³, C. J. O. Reichhardt³, and Yan Feng^{2 *}

¹ *School of Science, Nantong University, Nantong 226019, China*

² *Jiangsu Key Laboratory of Thin Films and Institute of Plasma Physics and Technology, School of Physical Science and Technology, Soochow University, Suzhou 215006, China*

³ *Theoretical Division, Los Alamos National Laboratory, Los Alamos, New Mexico 87545, USA*

** E-mail: liwei@ntu.edu.cn; fengyan@suda.edu.cn*

(Dated: October 6, 2022)

Collective transport properties of a one-dimensional asymmetric periodic substrate (1DAPS) modulated two-dimensional dusty plasma (2DDP) driven by an unbiased sinusoidal excitation force are investigated using Langevin dynamical simulations. It is discovered that, by changing the amplitude and frequency of the unbiased sinusoidal external excitations, as well as the depth of 1DAPS, both the direction and speed of the persistent particle flow can be adjusted, i.e., both the flow rectification and its reversal of the ratchet effect of the steady drift motion for particles are achieved using various excitations. For the studied 2DDP under the 1DAPS, when the amplitude of the excitation increases from zero, the magnitude of the overall drift velocity increases from zero to its first maximum in the easy direction of the 1DAPS, next decreases gradually back to zero, and then increases from zero to its second maximum in the hard direction of 1DAPS before finally gradually decaying. It is found that, as the frequency of the excitation and the depth of 1DAPS change, the maximum overall drift velocity also varies, and the corresponding magnitude of the excitation varies simultaneously. The observed ratchet effect in both the easy and hard directions of 1DAPS for 2DDP is attributed to the combination of the spatial symmetry breaking of 1DAPS and the inertial effects of particles, which is further confirmed by the three different presented diagnostics.

I. INTRODUCTION

When overdamped particles are modulated by an asymmetric periodic substrate, such as a series of sawtooth shaped potential wells, the so-called rocking ratchet effect can be exhibited, in which an applied ac drive generates a net dc flow of particles^{1,2}. If an asymmetric periodic substrate is flashed on and off in a system with thermal fluctuations, a flashing ratchet effect may still appear, even without an ac drive^{1,3}. Various ratchet effects have been studied in a wide variety of systems, including colloidal assemblies¹⁻³, biological systems⁴, magnets^{5,6}, cold atom arrays⁷, solid state devices^{8,9}, quantum systems^{10,11}, fluids on asymmetric substrates¹², superconducting vortices¹³, granular matter¹⁴ and active matter¹⁵. In these asymmetric substrate modulated systems, there is generally an easy flow direction for particles in which the force needed to move over the substrate barrier is smaller than that for the flow in the opposite or hard direction. In most ratchet systems, particle flows occur only in the easy direction; however, there are still some cases where the dc drift velocity undergoes a reversal under different conditions, so that particle flows may also preferentially occur in the hard direction. There may even be multiple reversals of the flow direction as a function of the ac driving amplitude, or the frequency, or the particle density¹⁶⁻²². These reversals may arise due to inertial effects²⁰ or collective effects¹⁶, in which localized quasiparticles appear or there are multiple effective species that experience inverted potentials²⁰⁻²².

One of the best studied examples of a particle-based

system coupled to a periodic asymmetric substrate that shows dc current reversals as a function of ac drive amplitude and particle density is vortices in type-II superconductors^{13,18-28}. The vortices behave like overdamped particles that have intermediate range interactions similar to the screened Coulomb interactions. At higher vortex densities, the system forms a triangular lattice, while at low vortex densities the system is in the liquidlike state. In the study of a two-dimensional (2D) assembly of superconducting vortices at a low density coupled to an asymmetric quasi-one dimensional (q1D) sawtooth potential¹³, it is found that under an ac drive, the vortices move in the easy flow direction of the substrate. Similar results are obtained for vortices in asymmetric channels¹⁴. In the experiment performed with superconducting vortices on asymmetric substrates²⁰, the vortex motion at low densities is in the easy direction as expected, but a reversal of the flow into the hard direction occurs as the vortex density increases, while for sufficiently large vortex densities, the dc flow disappears. The current reversals are attributed to the collective interactions between the vortices, since at high densities the system can be viewed as containing two effective species of particles. The second species interacts with the potential landscape created by the first species rather than directly experiencing the substrate asymmetry, and the asymmetry of this potential landscape is inverted as compared with the substrate asymmetry. In the study of a simpler version of the 2D superconducting vortex assembly on a q1D asymmetric potential²¹, it is found that at low densities, the ratchet motion is in the easy flow direction, in agreement with Ref.¹³; however, at higher drives

there is a reversal in the flow when two rows of vortices occupy each substrate minimum and undergo a buckling transition into one high density row and one low density row, effectively inverting the potential experienced by a portion of the vortices. In general, systems that show a ratchet reversal due to collective effects have an initial ratchet flow in the easy direction of the substrate for low ac drive amplitudes^{20,21,23,26,28}. A similar type of ratchet reversal is studied for superconducting vortex flows in 2D Josephson networks where a similar q1D asymmetric substrate potential arises²⁹. Studies of 2D active matter on 1D asymmetric substrates also show that at low densities the particle flow is in the easy direction, but when collective effects come into play, there can be a reversal in which the flow is in the hard direction²². Ratchet reversals may also arise in systems where inertial effects come into play^{17,30}.

Another particle-based system is dusty plasma^{31–40}, or complex plasma, where micron-sized dust particles absorb free electrons and ions in plasma, so that these dust particles become highly charged to $\sim -10^4 e$ typically in the steady state. In dusty plasmas, the interaction between dust particles is the Yukawa repulsion^{41,42}, and these particles are strongly coupled due to their high charges^{31–33,43}. Under typical laboratory conditions, due to the electric field in the sheath, dust particles can self-organize into a single layer suspension, either in the crystal or liquid state, i.e., two-dimensional dusty plasma (2DDP)^{33,44,45}. In dust plasma experiments, individual particle identification and tracking from video imaging can be achieved easily using high-speed cameras, due to the length scale of the interparticle distance and the time scale of the particle motion^{33,46–48}. Dusty plasmas are typically used to study a variety of fundamental physics procedures in solids and liquids at the individual particle level, such as phase transitions^{49–52}, transport^{38,45,53,54}, waves^{39,44,55,56}, and other dynamics^{57–60}. Unlike many other 2D strongly coupled systems such as charged colloids in solution or vortices in superconductors, the dust motion in the plasma environment is underdamped, so that inertial effects come into play, leading to the appearance of phonons^{56,61} and shock wave phenomena^{62–64}. The collective dynamics of dust particles can be modulated by applying substrates in experiments. For example, a stripe electrode is used to generate substrates to manipulate the transport of dust particles^{65,66}. Recently, using simulations, the dynamics of dusty plasma modulated by periodic substrates are extensively investigated, such as the depinning dynamics of 2DDP modulated by 1D and 2D periodic substrates^{67–70}. Studying the dynamics of dusty plasmas under substrates would also be useful for understanding phenomena in other particle systems where inertial effects could come into play, such as acoustically levitated particles⁷¹, certain active matter systems⁷², granular matter⁷³, and ions in trap arrays⁷⁴. Due to its suitable length and temporal scales, dusty plasma is a natural model system to explore ratchet effects in the presence of both collective interactions and

inertia.

In a recent experiment⁷⁵ performed in dusty plasma with a ring-shaped 1D dust particle chain confined inside an asymmetric-sawtooth-shaped channel, persistent flows of these dust particles are achieved. By changing the plasma conditions of the gas pressure or the plasma power, the direction of the dust particle flow is controlled. In combination with the corresponding numerical simulations, it is found that the asymmetric potential and collective effects are the two keys in the observed dusty plasma ratchet rectification and reversal. Other simulation results also show dusty plasma ratchet effects in a q1D asymmetric potential through measurements of the velocity distributions⁷⁶.

In this paper, using computer simulations, we investigate the collective transport of 2DDP under a one-dimensional asymmetric periodic substrate (1DAPS) driven by unbiased external excitations. The specified asymmetric periodic substrates are similar to the geometries studied in superconducting vortex systems^{21,27,29} or active matter systems²², but different from the geometry in Ref.⁷⁵. The rest of this paper is organized as follows. In Sec. II, we briefly introduce our simulation method to mimic 2DDP under ratchet substrates driven by unbiased external excitations. In Sec. III, we present our simulation results in details, and also provide our interpretation of these results. We compare our results with the previous findings in 2D overdamped systems of superconducting vortices and active matter under similar 1D asymmetric potentials, and also discuss the possible future extension of the current work. Finally, we provide a brief summary of our findings in Sec. IV.

II. SIMULATION METHOD

We use Langevin dynamical simulations to investigate the collective transport properties of a 1DAPS modulated 2DDP driven by unbiased external excitation forces. The equation of motion for the dust particle i is given by

$$m\ddot{\mathbf{r}}_i = -\nabla\Sigma\phi_{ij} - \nu m\dot{\mathbf{r}}_i + \xi_i(t) + \mathbf{F}_i^S + \mathbf{F}_i^D. \quad (1)$$

Here, $-\nabla\Sigma\phi_{ij}$ is the particle-particle interaction force, which has the form of a Yukawa or screened Coulomb potential $\phi_{ij} = Q^2 \exp(-r_{ij}/\lambda_D)/4\pi\epsilon_0 r_{ij}$, where Q is the particle charge, ϵ_0 is the permittivity of free space, r_{ij} is the distance between particles i and j , and λ_D is the environment parameter of the Debye screening length due to the free electrons and ions in plasma. The second term $-\nu m\dot{\mathbf{r}}_i$ is the frictional drag that is proportional to the particle velocity. The third term $\xi_i(t)$ is the Langevin random kicks, which are assumed to be Gaussian distributed with a mean of zero. According to the fluctuation-dissipation theorem^{77,78}, $\langle \xi_i(0)\xi_i(t) \rangle = 2\nu k_B T \delta(t)$, the magnitude $\xi_i(t)$ of the Langevin random kicks is related to the specified target temperature. The fourth term \mathbf{F}_i^S is the force from the applied 1DAPS,

which has the form

$$U(x) = U_0[\sin(2\pi x/w) + 1/4 \sin(4\pi x/w)], \quad (2)$$

so that $\mathbf{F}_i^S = -\frac{\partial U(x)}{\partial x} \hat{\mathbf{x}} = (-\pi U_0/w)[2 \cos(2\pi x/w) + \cos(4\pi x/w)] \hat{\mathbf{x}}$. Here, U_0 and w are the depth and width of the 1DAPS, in units of $E_0 = Q^2/4\pi\epsilon_0 a$ and a , respectively, where $a = (n\pi)^{-1/2}$ is the Wigner-Seitz radius for the areal number density n . The last term on the right-hand side of Eq. (1), $\mathbf{F}_i^D = F_A \sin(\omega t) \hat{\mathbf{x}}$, is the applied unbiased sinusoidal excitation force, which has a mean value of zero.

Typically, 2DDPs, or 2D Yukawa systems, are described using two dimensionless parameters, which are the coupling parameter Γ and the screening parameter κ ^{33,35,36,79,80}. These two dimensionless parameters are defined as $\Gamma = Q^2/(4\pi\epsilon_0 a k_B T)$ and $\kappa = a/\lambda_D$, respectively, where T is the dust particle kinetic temperature. From these definitions, the coupling parameter Γ can be regarded as the inverse temperature, and the screening parameter κ indicates the length scale of the space occupied by one dust particle, while the environment parameter of the Debye screening length λ_D is assumed to be constant. Here, we fix $\Gamma = 1000$ and $\kappa = 2$ for our simulated 2DDP, which corresponds to the typical solid or crystal state without any substrates or external excitations⁷⁹. To normalize the length, in addition to the Wigner-Seitz radius a , we also use the lattice constant b , the average distance between nearest neighbors. For a 2D defect-free triangular lattice we have $b = 1.9046a$. Time scales are normalized by the inverse nominal 2DDP frequency⁸⁰, $\omega_{pd}^{-1} = (Q^2/2\pi\epsilon_0 m a^3)^{-1/2}$, which is the typical time scale of interparticle collisions for strongly coupled 2DDP.

Our simulation includes 1024 particles within a rectangular box of dimensions $61.1a \times 52.9a$ with periodic boundary conditions. Since the simulated size in the x direction is $61.1a \approx 32.07b$, in order to satisfy the periodic boundary conditions, we set the width of the potential well of the substrate w to values that produce integer numbers of the potential well within the simulation box. Here, we set $w = 2.004b$, corresponding to 16 full potential wells in the x direction. For the depth of the 1DAPS, we specify four different values, $U_0/E_0 = 0.01, 0.05, 0.1$, and 0.2 , respectively. The expression of the external sinusoidal excitation force F_i^D in Eq. (1) has two parameters, the amplitude F_A and the angular frequency ω , which are measured in units of $F_0 = Q^2/4\pi\epsilon_0 a^2$ and ω_{pd} , respectively. We increase the amplitude of the sinusoidal excitation force F_A , and then measure the corresponding collective directional transport for different angular frequencies of $\omega/\omega_{pd} = 2\pi/140, 2\pi/70$, and $2\pi/35$, respectively. The frictional damping coefficient is set to $\nu = 0.027\omega_{pd}$ in order to mimic the typical experimental conditions⁸¹. As in Ref.⁸², we specify the cutoff radius of the Yukawa potential as $24.8a$. For each simulation run, we integrate Eq. (1) for $\geq 10^5$ steps with a time step of $0.0028\omega_{pd}^{-1}$ in order to reach a steady state, and then record the positions and velocities of all particles during

the next several hundred periods of the sinusoidal excitation force for the data analysis reported here. Other simulation details are similar to those described in Ref.⁸³. We also perform a few test runs for a much larger system containing 4096 particles to confirm no substantial differences from the results reported here.

III. RESULTS AND DISCUSSION

A. Structure of 2DDP on 1DAPS

We first focus on the structure or arrangement of the dust particles modulated by the applied 1DAPS with different depths of the potential well $U(x)$, in the absence of the excitation force. Figure 1 presents snapshots of the simulated particle positions under the 1DAPS with different values of U_0 , as well as sketches of the substrate potential. Clearly, the biharmonic function of $U(x)$ contains a single well or minimum in each spatial period, and the spatial asymmetry of the substrate $U(x)$ is present only in the x direction. To the left side of the minimum of the potential well the slope is gentle, while the right side is steep. In Fig. 1, the parameters for the 2DDP and the spatial period of the 1DAPS are fixed to $\Gamma = 1000$, $\kappa = 2$, and $w/b = 2.004$, while we vary only the substrate depth, as specified to $U_0/E_0 = 0.01, 0.05$, and 0.2 for Figs. 1(a), 1(b), and 1(c), respectively.

As shown in Fig. 1, when modulated by the applied 1DAPS with different depths, the simulated particles exhibit completely different arrangements. When the depth of the 1DAPS is shallow, such as $U_0/E_0 = 0.01$ in Fig. 1(a), the constraint from the substrate is negligible compared with the interparticle interaction, so that all particles form a nearly triangular floating solid lattice, independent of the locations of the potential wells of the 1DAPS. When the substrate depth increases to $U_0/E_0 = 0.05$ as shown in Fig. 1(b), each potential well of the 1DAPS captures two ordered rows of particles that are aligned with the substrate potential. One row is at the minimum of the potential well, while the other is not, resulting in a pinned smectic state, different from the arrangement of particles modulated by symmetric substrates⁶⁸. Within each potential well, the particles adopt a stable zigzag arrangement to reduce the interparticle interactions. For the deeper substrate of $U_0/E_0 = 0.2$ in Fig. 1(c), two distinctive rows of particles with different number densities appear in each 1DAPS potential well. The row on the steep side of the potential well contains many more particles than the other row, which is also closer to the potential minimum, due to the stronger trapping by the steep side of the substrate. Clearly, as the depth of the 1DAPS becomes larger, the arrangement of particles exhibits a more pronounced asymmetry in the direction of the 1DAPS constraint. This structural transition is caused by the competition between the particle-particle interactions and the particle-substrate interaction. The structures in Fig. 1 can be compared to the

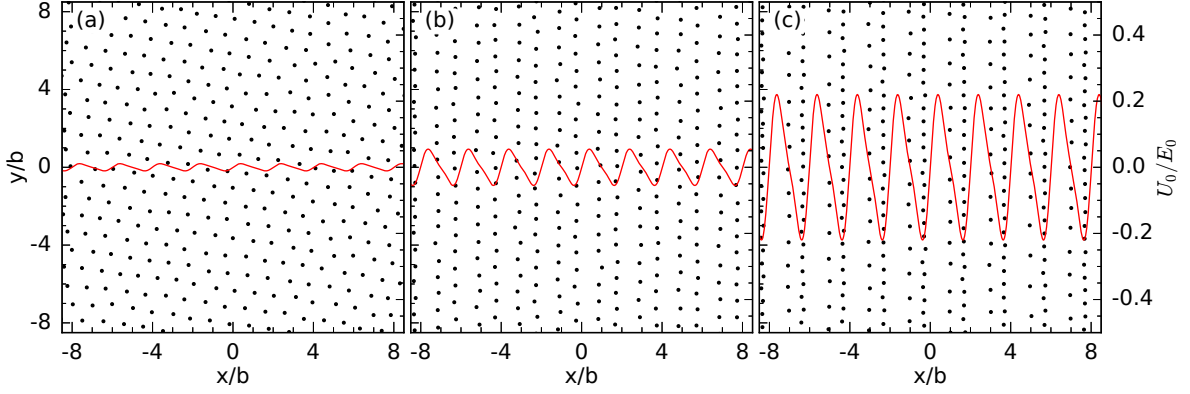


FIG. 1. Snapshots of the particle positions (dots) of a 2DDP under the 1DAPS (curve) of $U(x) = U_0[\sin(2\pi x/w) + 1/4 \sin(4\pi x/w)]$ with various substrate depths U_0/E_0 of 0.01 (a), 0.05 (b), and 0.2 (c). The conditions of the simulated 2DDP are $\Gamma = 1000$ and $\kappa = 2$, corresponding to a solid state. When $U_0/E_0 = 0.01$ in panel (a), the particles are uniformly distributed in a triangular lattice, independent of the locations of the potential wells of the 1DAPS. When $U_0/E_0 = 0.05$ in panel (b), two rows of particles sit in a stable zigzag arrangement within each potential well of the 1DAPS, forming a zigzag structure. When $U_0/E_0 = 0.2$ in panel (c), the two particle rows in each potential well become highly asymmetric, and the row at the bottom of the potential well contains many more particles than the other row. Note, only $\approx 32\%$ of the total simulation box is plotted here.

ordering of 2D superconducting vortex assemblies under similar 1D asymmetric substrates²¹, where for intermediate substrate depths there are two rows of particles in each potential minimum similar to Fig. 1(b), while for large substrate depths each minimum contains one dense row and one sparse row, just like Fig. 1(c).

B. Bidirectional flow with varying depths of 1DAPS

To study the effect of the unbiased sinusoidal excitation force on the transport of a 1DAPS modulated 2DDP, we calculate the overall drift velocity V for all particles. Since both the 1DAPS and the external sinusoidal excitation force are only in the x direction, the overall drift velocity in the y direction should be always around zero under all studied conditions, which is confirmed in fact. Thus, we focus only on V_x , the overall drift velocity in the x direction, averaged over two hundred periods of the external sinusoidal excitation force using

$$V_x = \langle N^{-1} \sum_{i=1}^N (\mathbf{v}_i \cdot \hat{\mathbf{x}}) \rangle, \quad (3)$$

as presented in Fig. 2. Clearly, from the specified 1DAPS in Fig. 1, the negative values of V_x in Fig. 2 correspond to drift motion in the easy direction of the 1DAPS, while the positive values of V_x indicate motion in the hard direction. Here, we vary the amplitude and angular frequency of the external sinusoidal excitation force for various substrate depths $U_0/E_0 = 0.01, 0.05, 0.1$, and 0.2 .

As the major result in this paper, we discover that the unbiased sinusoidal excitation force induces an overall drift flow of 2DDP in both the easy and hard direc-

tions of the 1DAPS, i.e., bidirectional flow. As presented in Fig. 2, the direction and magnitude of the overall drift velocity are modified by changing the depth of the 1DAPS and the amplitude of the unbiased external sinusoidal excitation force F_A . For the shallowest substrate of $U_0/E_0 = 0.01$, the system forms a triangular lattice that floats above the substrate, due to the tiny constraint from the 1DAPS. Thus, all particles move nearly rigidly back and forth under unbiased external excitations, resulting in a nearly zero net dc drift, as shown in Fig. 2. From Fig. 2, when the substrate is deeper $U_0/E_0 \geq 0.05$, the particle arrangements are modulated by the 1DAPS, leading to a significant ratchet effect under the application of sinusoidal excitation forces. As the amplitude of the sinusoidal excitation F_A increases from zero, the overall drift velocity V_x first gradually increases from zero in the easy direction of the 1DAPS to its maximum value, then gradually decreases in magnitude back to zero. As F_A further increases, the drift velocity V_x reverses toward the steeper side of the 1DAPS, i.e., the hard direction, and increases to its maximum, then finally decays gradually when F_A is large enough. From Fig. 2, clearly, as the substrate depth U_0 increases, the ratchet effect is more significant, with higher peak values in both the easy and hard directions. In Fig. 2, it seems that, when the ratchet flow reversal occurs, the corresponding excitation amplitude F_A also increases with the depth U_0 of the 1DAPS.

C. Interpretation of bidirectional flow

We attribute the observed ratchet effect in both the easy and hard directions to the combination of the spatial symmetry breaking of the 1DAPS and the inertial effects of the particles, as described in detail below. In

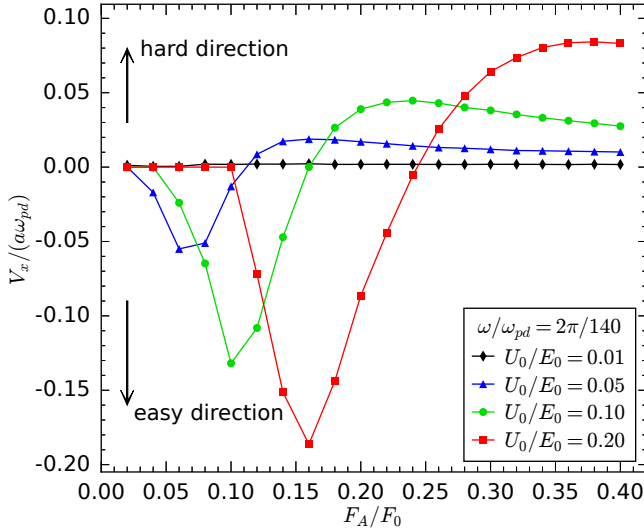


FIG. 2. Calculated overall drift velocity V_x of all simulated particles in a 2DDP with $\Gamma = 1000$ and $\kappa = 2$, as a function of the amplitude of the sinusoidal excitation force F_A , with the fixed angular frequency $\omega/\omega_{pd} = 2\pi/140$, for different substrate depths of $U_0/E_0 = 0.01, 0.05, 0.10$, and 0.20 . For the shallowest substrate of $U_0/E_0 = 0.01$, $V_x \approx 0$ for all values of F_A . For $U_0/E_0 = 0.05, 0.1$, and 0.2 , as F_A increases gradually from zero, V_x initially increases in magnitude with F_A to a maximum value in the $-x$ direction, next decreases in magnitude back to zero, and then increases again to a maximum in the $+x$ direction before decaying gradually. Thus, we find both a rectification of the particle motion and a reversal of the ratchet flow. The direction and magnitude of the overall drift flow velocity are both controlled by the depth of the 1DAPS and the amplitude of the unbiased sinusoidal excitation force.

Fig. 2, the overall drift motion in the easy direction can be explained by the spatial symmetry breaking of the 1DAPS. When the amplitude of the sinusoidal excitation F_A is small, it is much easier for particles to move along the gentle side of each potential well than the steep side to cross the potential barrier of the substrate, leading to a diode-like effect. As a result, a higher probability for motion along the gentle side leads to an overall drift motion in the easy direction of the 1DAPS, i.e., the $-x$ direction. As the excitation amplitude F_A increases gradually, more particles are able to leap over the potential barrier of the substrate along the easy direction of the 1DAPS, naturally leading to an increase of the overall drift velocity. In fact, if the excitation amplitude F_A increases further, more particles are also able to go beyond the potential barrier along the hard direction as well, and as a result, the diode-like effect may be reduced. Within this range of the excitation amplitude F_A , clearly there is a peak in the magnitude of V_x for motion in the $-x$ or easy direction, which occurs at $F_A/F_0 = 0.06, 0.10$, and 0.16 for $U_0/E_0 = 0.05, 0.10$, and 0.20 , respectively, as shown in Fig. 2. When the excitation amplitude F_A further increases, the overall drift velocity V_x is still in the easy direction; however, its magnitude gradually decays

until reaching zero.

If there were no inertia or other collective effects, this would be the end of the story and the ratchet effect would disappear for higher values of F_A . Instead, however, we find a reversal of the ratchet motion in the hard direction accompanied by the appearance of a second peak in the magnitude of V_x as F_A increases further.

Indeed, the relative steepness of the decrease in V_x from its negative peak value in Fig. 2 already indicates that an additional mechanism has come into play beyond the simple difference in the depinning threshold for motion in the easy and hard directions. This mechanism is the emergence of a lag in the response due to the presence of inertia in the dynamics of the simulated particles. When the sinusoidal excitation force reverses its direction from the $+x$ to the $-x$ direction, there is an overshoot in the motion of the particles due to the particle inertia, suggesting that the particles are unable to reverse their direction of motion immediately but instead continue moving in the $+x$ direction over a specific distance δd to reduce their velocity to zero, then begin to move in the $-x$ direction again. Clearly, the magnitude of δd increases with F_A until eventually it is the same size as the width of the steep side of the potential. When this happens, particles are carried over the barrier in the hard direction due to inertia alone. Since the distance from the potential well minimum to the edge of the well in the easy flow direction is longer, the inertia is insufficient to push the particles over the barrier in the easy direction. In essence, the presence of inertia causes a lag in the response of the particles to the external sinusoidal excitation force, resulting in a hysteretic behavior in the response of the particle velocity. A steep tilt of the ratchet potential corresponds to a large hysteresis loop, which results in a positive overall drift velocity.

Now let us choose the condition of $U_0/E_0 = 0.10$ in Fig. 2 to explore the mechanism of the variation of V_x with the amplitude of the sinusoidal excitation force F_A . For small amplitudes of the external sinusoidal excitation force, such as $F_A/F_0 = 0.02$ or 0.04 for the 2DDP system with $U_0/E_0 = 0.10$, the coupled particles are pinned at the bottom of the potential wells and most cannot overcome the potential barriers, leading to a collective overall drift velocity $V_x \approx 0$. As the amplitude of the external sinusoidal excitation force increases from $F_A/F_0 = 0.04$ to 0.1 , more and more particles have enough energy to leap over the potential barrier in the easy direction of the 1DAPS, leading to an increase of the overall drift velocity in the easy direction. When the amplitude of the external sinusoidal excitation force further increases from $F_A/F_0 = 0.1$ to ≈ 0.24 , the competition between the directional probability and the hysteresis due to inertial effects determines the overall net transport direction of particles. As the excitation force amplitude F_A further increases, the directional probability effect decreases and the hysteresis effect increases, so a reversal of the overall drift motion occurs. As F_A/F_0 increases further well beyond 0.24 , the amplitude of the external sinusoidal ex-

citation force becomes large enough that the selective role of the ratchet potential drops slowly, so that the overall net collective drift velocity decreases gradually to zero.

D. Diagnostics to support interpretation

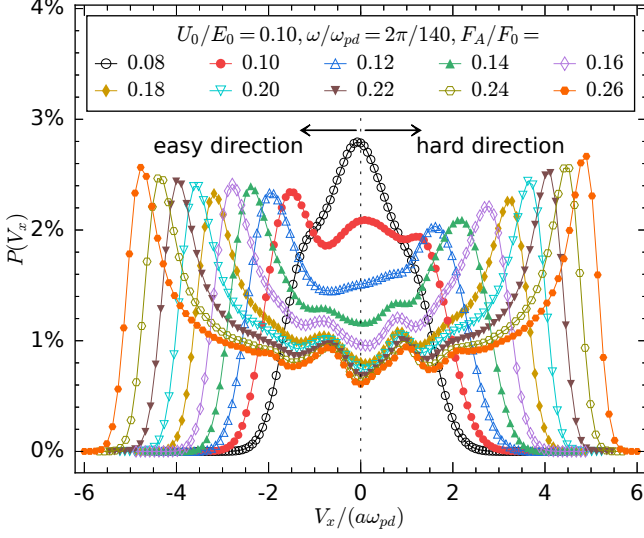


FIG. 3. Calculated velocity distribution $P(V_x)$ of the particle motion for various excitation force amplitudes F_A at fixed frequency $\omega/\omega_{pd} = 2\pi/140$ under the 1DAPS depth $U_0/E_0 = 0.1$. For the lower amplitudes $F_A/F_0 \leq 0.14$, the probability of particles with negative values of V_x is larger than that for positive values of V_x , indicating that particles are more likely to climb the potential barrier along the gentle side of 1DAPS, i.e., the easy direction. For the higher amplitudes $F_A/F_0 \geq 0.18$, the height of the positive velocity peak in $P(V_x)$ is significantly higher than that of the negative velocity peak, indicating that the overall drift velocity changes to the hard direction.

To further confirm our interpretation above about the mechanism of the excitation induced drift flow in both the easy and hard directions of all particles under the 1DAPS, we analyze the velocity distribution $P(V_x)$. In Fig. 3, we plot our calculated $P(V_x)$ versus V_x under the condition of $U_0/E_0 = 0.1$ for our studied system in Fig. 2 with varying F_A values. Clearly, when $F_A/F_0 = 0.08$, $P(V_x)$ presented in Fig. 3 has a prominent peak at $V_x = 0$, and the total distribution $P(V_x)$ of $V_x < 0$ is slightly greater than that of $V_x > 0$, resulting in a net drift velocity in the $-x$ direction. For $F_A/F_0 = 0.1$, where the maximum magnitude of the easy direction ratcheting motion occurs, there are two peaks in $P(V_x)$ near $V_x = \pm 1.5a\omega_{pd}$, but the peak for motion in the $-x$ direction is much higher than that for motion in the $+x$ direction, indicating that more particles climb along the easy direction of the 1DAPS than along the hard direction, naturally leading to an overall drift in the easy direction. As F_A further increases, the peak at $V_x = 0$

diminishes and velocity peaks appear only at finite positive and negative velocities, with the magnitude of the positive velocity peak increasing substantially with increasing F_A . When $F_A/F_0 \geq 0.18$, the height of the positive velocity peak is significantly higher than that of the negative velocity peak, indicating that the overall drift velocity changes to the hard direction, agreeing well with the V_x results in Fig. 2. Clearly, there are also several smaller peaks near $V_x = \pm a\omega_{pd}$, likely the result of collective effects, that do not contribute much to the overall drift velocity V_x .

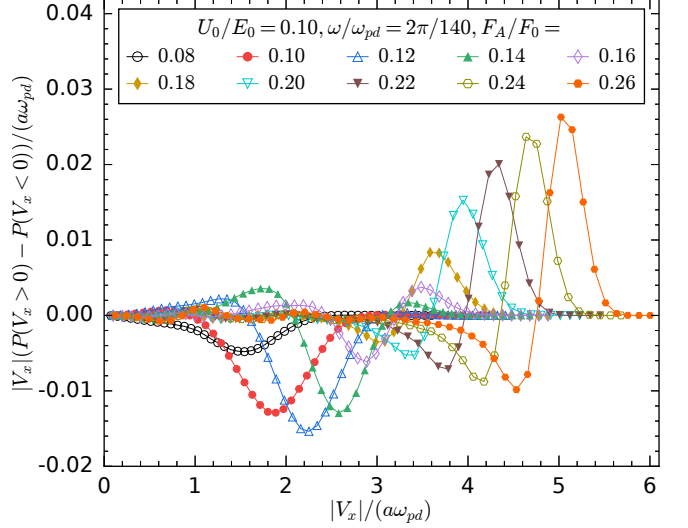


FIG. 4. Calculated probability current of particle motion $|V_x|(P(V_x > 0) - P(V_x < 0))$ as a function of the speed $|V_x|$, for various excitation forces under fixed conditions of $U_0/E_0 = 0.10$ and $\omega/\omega_{pd} = 2\pi/140$. When the excitation force amplitude is small, $F_A/F_0 \leq 0.12$, the negative peak of the probability current increases gradually with F_A , resulting in an increase in the overall drift velocity V_x in the $-x$ direction, corresponding to a larger number of particles moving across the potential barrier in the easy direction. When $0.14 \leq F_A/F_0 \leq 0.16$, the magnitude of the negative velocity peak of the probability current decreases gradually with F_A , while a peak at positive velocities appears and increases gradually with F_A , corresponding to more particles climbing the potential barrier along the steep side of the 1DAPS. When $F_A/F_0 \geq 0.18$, the sinusoidal excitation force becomes large enough to drive all particles to climb the steep side of the 1DAPS, so that the positive velocity peak of the probability current increases significantly with the excitation amplitude F_A , leading to a net current in the $+x$ direction. This net flow direction is controlled by the asymmetry of the substrate and the amplitude of the unbiased excitation force.

In Fig. 4 we present the calculated probability current of particle motion as a function of the speed $|V_x|$ for various excitation forces with different amplitudes F_A in our simulated 2DDP system with a ratchet substrate of $U_0/E_0 = 0.10$. We obtain this quantity by multiplying $|V_x|$ by $(P(V_x > 0) - P(V_x < 0))$ for each value of $|V_x|$. For $F_A/F_0 \leq 0.12$, the net velocities are mainly negative,

while for $F_A/F_0 = 0.14$ to 0.16 , the system has a combination of both negative and positive velocities that add up to a value close to zero. When $F_A/F_0 \geq 0.18$, the probability current of the particle motion indicates that the net velocity is completely dominated by the substantial positive component of the velocity.

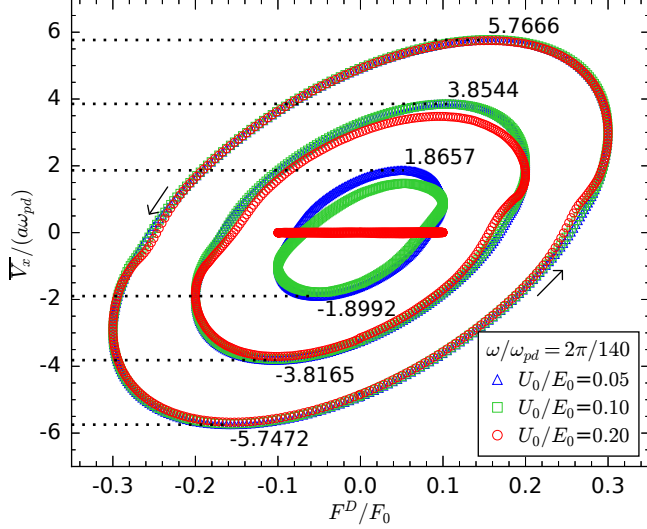


FIG. 5. Calculated instantaneous overall velocity \overline{V}_x averaged over all particles, as a function of the instantaneous magnitude of the sinusoidal excitation F^D , during only one period of the excitation force, as U_0/E_0 varies. The significant hysteresis in the \overline{V}_x versus F^D plot clearly indicates an overshoot effect due to the inertia of the particles. From inner to outer sets of curves, $F_A/F_0 = 0.1, 0.2$, and 0.3 .

In Fig. 5 we plot the instantaneous velocity averaged over all particles \overline{V}_x versus the instantaneous magnitude of the excitation force F^D at different values of F_A , during only one period of the excitation force, for different 1DAPS depths of $U_0/E_0 = 0.05, 0.10$, and 0.20 . When $F_A/F_0 = 0.1$, under the condition of $U_0/E_0 = 0.2$, almost all particles remain pinned, so that \overline{V}_x is nearly zero at all times. However, under the conditions of $U_0/E_0 = 0.05$ and 0.1 , the amplitude of $F_A/F_0 = 0.1$ is large enough to induce depinning, so that particles are able to move across the 1DAPS. For the conditions under which particles are able to move across the potential barrier of the 1DAPS, when the direction of the excitation force is reversed, the corresponding overall instantaneous velocity \overline{V}_x for all particles is not able to respond immediately due to the inertia, resulting in the appearance of hysteresis, also termed the overshoot effect⁶⁸. For $F_A/F_0 = 0.1$, the upper part of the cycle gradually increases in diameter as the depth of the 1DAPS decreases, indicating that more particles are able to cross the potential barrier on the steep side of the 1DAPS. For $F_A/F_0 = 0.2$, the cycle at $U_0/E_0 = 0.20$ encloses a slightly smaller area than the $U_0/E_0 = 0.05$ and $U_0/E_0 = 0.10$ cycles, suggesting that for $U_0/E_0 = 0.20$ some particles are not able to cross the barrier on the steep side of the 1DAPS,

leading to the maximum \overline{V}_x in the $+x$ direction below $3.8544a\omega_{pd}$, which is the maximum \overline{V}_x for $U_0/E_0 = 0.05$ or $U_0/E_0 = 0.10$. For $F_A/F_0 = 0.3$, the extreme values of \overline{V}_x for all the cycles at different depths of 1DAPS are nearly the same in the easy and hard directions, indicating that all of the particles are able to cross the potential barrier in both the $\pm x$ directions, leading to an overall net flow in the hard direction since the maximum peak in the hard direction of $\overline{V}_x = 5.7666a\omega_{pd}$ is slightly larger.

Clearly, from our calculated velocity distribution $P(V_x)$ in Fig. 3, probability current $|V_x|(P(V_x > 0) - P(V_x < 0))$ in Fig. 4, and instantaneous overall velocity \overline{V}_x versus F^D in Fig. 5 presented above, we further confirm our interpretation of the observed ratchet effect for bidirectional flow of the particle motion. In our interpretation, the spatial symmetry breaking of the 1DAPS mainly induces a collective drift motion of particles in the easy direction of the 1DAPS when the amplitude of the excitation is small; however, when the amplitude of the excitation is large enough, the collective drift motion of particles in the hard direction is mainly caused by the combination of inertial effects of the particles and the spatial symmetry breaking of the 1DAPS. Our results presented above clearly indicate that the depth of the 1DAPS and the amplitude of the excitation can be used to modify the direction and magnitude of the overall drift flow. The next question is then whether the frequency of the excitation is also able to modify the overall drift velocity direction, as we study next.

E. Bidirectional flow with varying frequencies of excitations

In Fig. 6 we present our calculated overall drift velocity V_x of our simulated 2DDP under an unbiased external sinusoidal excitation force with varying amplitudes F_A and three different angular frequencies $\omega/\omega_{pd} = 2\pi/140, 2\pi/70$, and $2\pi/35$, with the unchanged depth $U_0/E_0 = 0.1$ of the 1DAPS. For each angular frequency, as F_A increases from zero, the overall drift velocity V_x always first increases in magnitude from zero to a maximum in the $-x$ direction, next gradually decreases back to zero, and then increases again to a maximum in the $+x$ direction before finally decaying gradually. This variation trend of V_x is very similar to that in Fig. 2. Clearly, for one specified 1DAPS, the direction and magnitude of the overall drift velocity can be adjusted by changing the amplitude F_A and frequency ω of the excitation force. From our interpretation, the underlying mechanism of the bidirectional flow in Fig. 6 should be the same as that in Fig. 2, which is the combination of the spatial symmetry breaking of the 1DAPS and the inertial effects of the particles. From Fig. 6, as the frequency of the excitation force increases, the maximum magnitude of the overall directional flow is reduced, probably because the particles do not have enough time to respond to the variation of the excitation force. For a fixed excitation force amplitude,

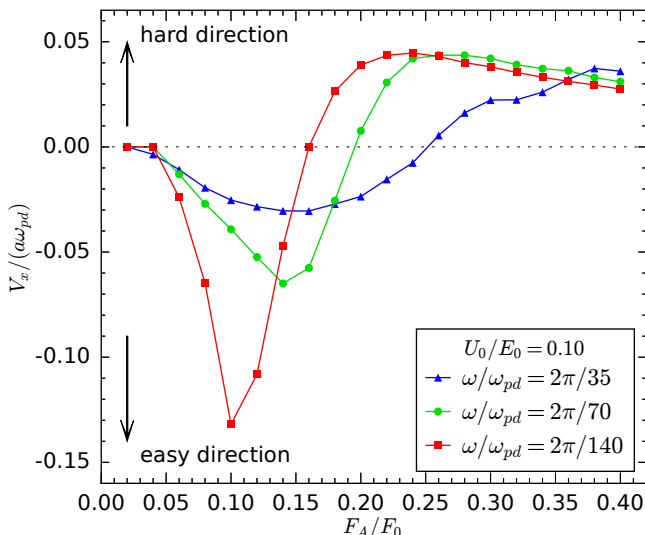


FIG. 6. Calculated overall drift velocity V_x of particles as a function of the excitation force amplitude F_A with different angular frequencies $\omega/\omega_{pd} = 2\pi/140$, $2\pi/70$, and $2\pi/35$, under the condition of unchanged substrate depth $U_0/E_0 = 0.1$. For all three presented frequencies, as the amplitude F_A of the excitation force gradually increases from zero, the overall drift velocity V_x first increases from zero to its maximum in the $-x$ direction, next gradually decreases to zero, and then increases again to its another maximum in the $+x$ direction until it finally decays gradually. For one specific excitation force amplitude, the magnitude and the direction of the overall drift velocity V_x are both determined by the excitation frequency ω . That is to say, the flow rectification and its reversal can also be achieved by adjusting the frequency of the excitation force.

the magnitude and direction of the overall drift velocity V_x of the particles are both determined by the excitation force frequency ω . In short, the flow rectification and its reversal of the overall drift velocity for all particles can be achieved by adjusting the excitation force frequency and amplitude.

F. Discussion

We would like to compare our results with the previous findings of superconducting vortices and active matter in 2D overdamped systems under similar 1D asymmetric potentials^{21,22,29}. In such systems, at low densities the collective effects are minimal and there is only one row or a partial row of particles in each periodic potential minimum. As an ac drive of increasing amplitude is applied, the system is first in a pinned phase. A transition occurs to finite dc flows in the easy direction of the substrate, while for larger ac drives, the dc flow drops back to zero. At higher densities, where two or more rows can fit in each potential minimum similar to what is shown in Fig. 1(b, c), the pinned phase is followed by finite dc flows in the hard direction of the substrate which reverse

at higher ac drive amplitudes to a dc flow in the easy direction of the substrate. The reversal results when there is a buckling of the type illustrated in Fig. 1(c) in the row of particles in each potential minimum, so that a dense row and a sparse row coexist in a single substrate minimum. Under ac excitations, the particles in the sparse row are more mobile and experience both the substrate potential and the effective substrate potential induced by the repulsion from the dense row of particles. Since the dense row is on the steep side of the potential minimum, it creates a steep barrier for the particles in the sparse row to jump out of the weaker side of the neighboring substrate potential. In contrast, the particles in the sparse row can push a portion of the particles in the dense row over the shorter but steeper side of the potential barrier, causing the particles in the dense row to perform a hop in the hard flow direction. At higher ac drives, all of the particles can overcome the potential barrier, and the flow transitions to regular ratchet motion in the easy direction.

Ratchet reversals are observed for other collective ratchet systems when the collective interactions lead to the emergence of two effective species of particles. The less strongly pinned species experiences a substrate potential that is effectively inverted, and this species undergoes ratcheting motion in the hard direction for lower ac drives, while at higher ac drives, the noninverted potential dominates and the ratcheting motion switches into the easy direction^{18,19,23,26}. This behavior is completely opposite from what we observe in Fig. 2. This suggests that although collective effects could still be occurring in the dusty plasma system, the ratchet reversal is primarily due to the inertial effects. For particles under a similar 1D asymmetric potential, it is found that in the overdamped limit the ratchet flow was only in the easy direction; however, in an underdamped system the ratchet motion occurs in the easy direction for small ac drives but reverses to the hard direction at higher ac drives³⁰, similar to what we observe in Fig. 2.

The dusty plasma ratchet effect we study opens several different future directions. Many other types of asymmetric potentials could be created that may lead to ratchet effects, such as 2D asymmetric sites^{18,19}, asymmetric confining walls^{20,23,26}, and even systems with frictional gradients²⁸. Since the ratchet effect depends on both the coupling strength and the inertia, it could be possible to create dust sorting devices where particles of different mass move in opposite directions or at different speeds. If a magnetic field is applied to the dusty plasma⁸⁴, gyroscopic effects may emerge similar to those found for skyrmions, and distinctive Magnus ratchet effects could appear^{85–87}. Since thermal effects are important, it should also be possible to create a flashing ratchet where the substrate is turned off and on to see whether there is directed motion^{1,3}. This would be most effective in the case where the system is fluid like or near the solid to liquid transition.

IV. SUMMARY

In summary, we discover the bidirectional flow of a 1DAPS modulated 2DDP driven by unbiased sinusoidal excitation forces using Langevin dynamical simulations. In the absence of the excitation force, the arrangement of the 2DDP is modulated by the 1DAPS. If the 1DAPS is shallow, the arrangement of the 2DDP is nearly unchanged from the typical triangular lattice. When the depth of the 1DAPS is deeper, within each potential well, there are two rows of particles forming a zigzag structure. When the depth of the 1DAPS is further increased, the two rows within one potential well become asymmetric, where one is dense and close to the bottom of the potential well, while the other is sparse and sitting on the gentle side of the potential well. After applying a sinusoidal excitation force to the 1DAPS modulated 2DDP, we find a particle flow rectification and its reversal while changing the amplitude of the excitation force. As the amplitude of the excitation force increases from zero, the overall drift velocity of the 2DDP first increases in magnitude from zero to a maximum in the easy direction of the 1DAPS, next gradually decreases back to zero, and then increases again to a maximum in the hard direction before finally decaying gradually. The magnitude of

the ratchet effect increases with the depth of the 1DAPS, and the maximum of the ratchet effect shifts to higher values of the amplitude of the excitation force. Furthermore, the frequency of the excitation force can be used to modify the magnitude of the ratchet effect and the location of the transition of the flow direction. We attribute the observed ratchet effect in both the easy and hard directions to the combination of the spatial symmetry breaking of the 1DAPS and the inertial effects of the particles, as further confirmed by the three different presented diagnostics.

V. ACKNOWLEDGMENTS

Work in China was supported by the National Natural Science Foundation of China under Grants Nos. 12105147 and 12175159, startup funds from Nantong University, and Innovation and Entrepreneurship Program of Jiangsu Province. Work at LANL was supported by the U. S. Department of Energy through the Los Alamos National Laboratory. Los Alamos National Laboratory is operated by Triad National Security, LLC, for the National Nuclear Security Administration of the U. S. Department of Energy (Contract No. 892333218NCA000001).

-
- ¹ P. Reimann, “Brownian motors: noisy transport far from equilibrium,” *Phys. Rep.* **361**, 57–265 (2002).
 - ² A. V. Arzola, K. Volke-Sepúlveda, and J. L. Mateos, “Experimental control of transport and current reversals in a deterministic optical rocking ratchet,” *Phys. Rev. Lett.* **106**, 168104 (2011).
 - ³ J. Rousselet, L. Salome, A. Ajdari, and J. Prost, “Directional motion of Brownian particles induced by a periodic asymmetric potential,” *Nature (London)* **370**, 446–448 (1994).
 - ⁴ B. Lau, O. Kedem, J. Schwabacher, D. Kwasnieski, and E. A. Weiss, “An introduction to ratchets in chemistry and biology,” *Mater. Horiz.* **3**, 310–318 (2017).
 - ⁵ A. Pérez-Junquera, V. I. Marconi, A. B. Kolton, L. M. Álvarez-Prado, Y. Souche, A. Alija, M. Vélez, J. V. Anguita, J. M. Alameda, J. I. Martín, and J. M. R. Parrondo, “Crossed-ratchet effects for magnetic domain wall motion,” *Phys. Rev. Lett.* **100**, 037203 (2008).
 - ⁶ J. H. Franken, H. J. M. Swagten, and B. Koopmans, “Shift registers based on magnetic domain wall ratchets with perpendicular anisotropy,” *Nature Nanotechnol.* **7**, 499–503 (2012).
 - ⁷ P. H. Jones, M. Goonasekera, and F. Renzoni, “Rectifying fluctuations in an optical lattice,” *Phys. Rev. Lett.* **93**, 073904 (2004).
 - ⁸ E. M. Roeling, W. Chr. Germs, B. Smalbrugge, E. J. Geluk, T. de Vries, R. A. J. Janssen, and M. Kemerink, “Organic electronic ratchets doing work,” *Nature Mater.* **10**, 51–55 (2011).
 - ⁹ C. Grossert, M. Leder, S. Denisov, P. Hänggi, and M. Weitz, “Experimental control of transport resonances in a coherent quantum rocking ratchet,” *Nature Commun.* **7**, 10440 (2016).
 - ¹⁰ H. Linke, T. E. Humphrey, A. Lofgren, A. O. Sushkov, R. Newbury, R. P. Taylor, and P. Omling, “Experimental tunneling ratchets,” *Science* **286**, 2314–2317 (1999).
 - ¹¹ T. Salger, S. Kling, T. Hecking, C. Geckeler, L. Morales-Molina, and M. Weitz, “Directed transport of atoms in a Hamiltonian quantum ratchet,” *Science* **326**, 1241–1243 (2009).
 - ¹² G. Lagubeau, M. Le Merrer, C. Clanet, and D. Quéré, “Leidenfrost on a ratchet,” *Nature Phys.* **7**, 395–398 (2011).
 - ¹³ C. S. Lee, B. Jankó, I. Derényi, and A. L. Barabási, “Reducing vortex density in superconductors using the ‘ratchet effect’,” *Nature (London)* **400**, 337–340 (1999).
 - ¹⁴ J. F. Wambaugh, C. Reichhardt, and C. J. Olson, “Ratchet-induced segregation and transport of nonspherical grains,” *Phys. Rev. E* **65**, 031308 (2002).
 - ¹⁵ C. J. Olson Reichhardt and C. Reichhardt, “Ratchet effects in active matter systems,” *Ann. Rev. Condens. Matter Phys.* **8**, 51–75 (2017).
 - ¹⁶ I. Derényi and T. Vicsek, “Cooperative transport of Brownian particles,” *Phys. Rev. Lett.* **75**, 374–377 (1995).
 - ¹⁷ J. L. Mateos, “Chaotic transport and current reversal in deterministic ratchets,” *Phys. Rev. Lett.* **84**, 258–261 (2000).
 - ¹⁸ C. C. de Souza Silva, J. V. de Vondel, M. Morelle, and V. V. Moshchalkov, “Controlled multiple reversals of a ratchet effect,” *Nature (London)* **440**, 651–654 (2006).
 - ¹⁹ W. Gillijns, A. V. Silhanek, V. V. Moshchalkov, C. J. Olson Reichhardt, and C. Reichhardt, “Origin of reversed vortex

- ratchet motion,” *Phys. Rev. Lett.* **99**, 247002 (2007).
- 20 J. E. Villegas, S. Savel’ev, F. Nori, E. M. Gonzalez, J. V. Anguita, R. García, and J. L. Vicent, “A superconducting reversible rectifier that controls the motion of magnetic flux quanta,” *Science* **302**, 1188–1191 (2003).
 - 21 Q. Lu, C. J. Olson Reichhardt, and C. Reichhardt, “Reversible vortex ratchet effects and ordering in superconductors with simple asymmetric potential arrays,” *Phys. Rev. B* **75**, 054502 (2007).
 - 22 D. McDermott, C. J. Olson Reichhardt, and C. Reichhardt, “Collective ratchet effects and reversals for active matter particles on quasi-one-dimensional asymmetric substrates,” *Soft Matter* **12**, 8606–8615 (2016).
 - 23 C. J. O. Reichhardt and C. Reichhardt, “Rectification and flux reversals for vortices interacting with triangular traps,” *Physica C* **432**, 125–132 (2005).
 - 24 K. Yu, T. W. Heitmann, C. Song, M. P. DeFeo, B. L. T. Plourde, M. B. S. Hesselberth, and P. H. Kes, “Asymmetric weak-pinning superconducting channels: Vortex ratchets,” *Phys. Rev. B* **76**, 220507 (2007).
 - 25 C. J. Olson Reichhardt and C. Reichhardt, “Commensurability, jamming, and dynamics for vortices in funnel geometries,” *Phys. Rev. B* **81**, 224516 (2010).
 - 26 D. Perez de Lara, M. Erekhinsky, E. M. Gonzalez, Y. J. Rosen, I. K. Schuller, and J. L. Vicent, “Vortex ratchet reversal: Role of interstitial vortices,” *Phys. Rev. B* **83**, 174507 (2011).
 - 27 V. A. Shklovskij, V. V. Sosedkin, and O. V. Dobrovolskiy, “Vortex ratchet reversal in an asymmetric washboard pinning potential subject to combined dc and ac stimuli,” *J. Phys.: Condens. Matter* **26**, 025703 (2014).
 - 28 C. Reichhardt, D. Ray, and C. J. Olson Reichhardt, “Reversible ratchet effects for vortices in conformal pinning arrays,” *Phys. Rev. B* **91**, 184502 (2015).
 - 29 V. I. Marconi, “Rocking ratchets in two-dimensional Josephson networks: Collective effects and current reversal,” *Phys. Rev. Lett.* **98**, 047006 (2007).
 - 30 B.-Q. Ai and F.-G. Li, “Transport of underdamped active particles in ratchet potentials,” *Soft Matter* **13**, 2536–2542 (2017).
 - 31 J. H. Chu and L. I, “Direct observation of Coulomb crystals and liquids in strongly coupled rf dusty plasmas,” *Phys. Rev. Lett.* **72**, 4009–4012 (1994).
 - 32 H. Thomas, G. E. Morfill, V. Demmel, J. Goree, B. Feuerbacher, and D. Möhlmann, “Plasma crystal: Coulomb crystallization in a dusty plasma,” *Phys. Rev. Lett.* **73**, 652–655 (1994).
 - 33 G. E. Morfill and A. V. Ivlev, “Complex plasmas: An interdisciplinary research field,” *Rev. Mod. Phys.* **81**, 1353–1404 (2009).
 - 34 V. E. Fortov, A. V. Ivlev, S. A. Khrapak, A. G. Khrapak, G. E. Morfill, “Complex(dusty) plasmas: Current status, open issues, perspectives,” *Phys. Rep.* **421**, 1–103 (2005).
 - 35 M. Bonitz, C. Henning, and D. Block, “Complex plasmas: a laboratory for strong correlations,” *Rep. Prog. Phys.* **73**, 066501 (2010).
 - 36 R. L. Merlino and J. A. Goree, “Dusty plasmas in the laboratory, industry, and space,” *Phys. Today* **57**, 32 (2004).
 - 37 A. Melzer, A. Homann, and A. Piel, “Experimental investigation of the melting transition of the plasma crystal,” *Phys. Rev. E* **53**, 2757 (1996).
 - 38 V. Nosenko and J. Goree, “Shear flows and shear viscosity in a two-dimensional Yukawa system (Dusty plasma),” *Phys. Rev. Lett.* **93**, 155004 (2004).
 - 39 S. Nunomura, S. Zhdanov, D. Samsonov, and G. Morfill, “Wave spectra in solid and liquid complex(dusty) plasmas,” *Phys. Rev. Lett.* **94**, 045001 (2005).
 - 40 C. A. Knapek, D. Samsonov, S. Zhdanov, U. Konopka, and G. E. Morfill, “Recrystallization of a 2D plasma crystal,” *Phys. Rev. Lett.* **98**, 015004 (2007).
 - 41 U. Konopka, G. E. Morfill, and L. Ratke, “Measurement of the interaction potential of microspheres in the sheath of a rf discharge,” *Phys. rev. Lett.* **84**, 891 (2000).
 - 42 J. Ashwin and A. Sen, “Microscopic origin of shear relaxation in a model viscoelastic liquid,” *Phys. Rev. Lett.* **114**, 055002 (2015).
 - 43 F. Wieben and D. Block, “Entropy measurement in strongly coupled complex plasmas,” *Phys. Rev. Lett.* **123**, 225001 (2019).
 - 44 P. Hartmann, Z. Donkó, T. Ott, H. Kählert, and M. Bonitz, “Magnetoplasmons in rotating dusty plasmas,” *Phys. Rev. Lett.* **111**, 155002 (2013).
 - 45 P. Hartmann, J. C. Reyes, E. G. Kostadinova, L. S. Matthews, T. W. Hyde, R. U. Masheyeva, K. N. Dzhumagulova, T. S. Ramazanov, T. Ott, H. Kählert, M. Bonitz, I. Korolov, and Z. Donkó, “Self-diffusion in two-dimensional quasimagnetized rotating dusty plasmas,” *Phys. Rev. E* **99**, 013203 (2019).
 - 46 L. I, W.-T. Juan, C.-H. Chiang, and J. H. Chu, “Microscopic particle motions in strongly coupled dusty plasmas,” *Science* **272**, 1626–1628 (1996).
 - 47 J. D. Williams, E. Thomas, L. Couëdel, A. V. Ivlev, S. K. Zhdanov, V. Nosenko, H. M. Thomas, and G. E. Morfill, “Kinetics of the melting front in two-dimensional plasma crystals: Complementary analysis with the particle image and particle tracking velocimetry,” *Phys. Rev. E* **86**, 046401 (2012).
 - 48 E. Thomas and J. Williams, “Experimental measurements of velocity dissipation and neutral-drag effects during the formation of a dusty plasma,” *Phys. Rev. Lett.* **95**, 055001 (2005).
 - 49 V. Nosenko, S. K. Zhdanov, A. V. Ivlev, C. A. Knapek, and G. E. Morfill, “2D melting of plasma crystals: Equilibrium and nonequilibrium regimes,” *Phys. Rev. Lett.* **103**, 015001 (2009).
 - 50 P. Hartmann, A. Douglass, J. C. Reyes, L. S. Matthews, T. W. Hyde, A. Kovács, and Z. Donkó, “Crystallization dynamics of a single layer complex plasma,” *Phys. Rev. Lett.* **105**, 115004 (2010).
 - 51 S. Singh, P. Bandyopadhyay, K. Kumar, and A. Sen, “Square lattice formation in a monodisperse complex plasma,” *Phys. Rev. Lett.* **129**, 115003 (2022).
 - 52 A. Melzer and A. Schella, “Instantaneous normal mode analysis of melting of finite dust clusters,” *Phys. Rev. Lett.* **108**, 225001 (2012).
 - 53 B. Liu and J. Goree, “Superdiffusion and Non-Gaussian statistics in a driven-dissipative 2D dusty plasma,” *Phys. Rev. Lett.* **100**, 05003 (2008).
 - 54 C. A. Romero-Talamás, E. M. Bates, W. J. Birmingham, and W. F. Rivera, “DPLX: Experiment to investigate heating and stability in magnetized rotating dusty plasmas,” *IEEE Trans. Plasma Sci.* **44**, 535 (2016).
 - 55 A. Piel, O. Arp, M. Klindworth, and A. Melzer, “Obliquely propagating dust-density waves,” *Phys. Rev. E* **77**, 026407 (2008).
 - 56 S. Nunomura, J. Goree, S. Hu, X. Wang, A. Bhattacharjee, and K. Avinash, “Phonon spectrum in a plasma crystal,” *Phys. Rev. Lett.* **89**, 035001 (2002).

- ⁵⁷ W. T. Yu, J. Cho, and J. C. Burton, "Extracting forces from noisy dynamics in dusty plasmas," *Phys. Rev. E* **106**, 035303 (2022).
- ⁵⁸ Y.-J. Lai and L. I, "Avalanche excitations of fast particles in quasi-2D cold dusty-plasma liquids," *Phys. Rev. Lett.* **89**, 155002 (2002).
- ⁵⁹ P. Hartmann, A. Zs. Kovács, A. M. Douglass, J. C. Reyes, L. S. Matthews, and T. W. Hyde, "Slow plastic creep of 2D dusty plasma solids," *Phys. Rev. Lett.* **113**, 025002 (2014).
- ⁶⁰ H.-W. Hu, Y.-C. Zhao, and L. I, "Avalanche structural rearrangements in cold dusty plasma liquids through cascaded coherent excitations of heterogeneous multiscale thermal acoustic waves," *Phys. Rev. Research* **4**, 023116 (2022).
- ⁶¹ L. Couëdel, V. Nosenko, S. K. Zhdanov, A. V. Ivlev, H. M. Thomas, and G. E. Morfill, "First direct measurement of optical phonons in 2D plasma crystals," *Phys. Rev. Lett.* **103**, 215001 (2009).
- ⁶² D. Samsonov, J. Goree, Z. W. Ma, A. Bhattacharjee, H. M. Thomas, and G. E. Morfill, "Mach cones in a Coulomb lattice and a dusty plasma," *Phys. Rev. Lett.* **83**, 3649–3652 (1999).
- ⁶³ J. Heinrich, S.-H. Kim, and R. L. Merlino, "Laboratory observations of self-excited dust acoustic shocks," *Phys. Rev. Lett.* **103**, 115002 (2009).
- ⁶⁴ A. Kananovich and J. Goree, "Shock width measured under liquid and solid conditions in a two-dimensional dusty plasma," *Phys. Rev. E* **104**, 055201 (2021).
- ⁶⁵ K. Jiang, Y. F. Li, T. Shimizu, U. Konopka, H. M. Thomas, and G. E. Morfill, "Controlled particle transport in a plasma chamber with striped electrode," *Phys. Plasmas* **16**, 123702 (2009).
- ⁶⁶ Y. F. Li, W. G. Zhang, J. X. Ma, K. Jiang, H. M. Thomas, and G. E. Morfill, "Traveling electric field probed by a fine particle above voltage-modulated strips in a striped electrode device," *Phys. Plasmas* **17**, 033705 (2010).
- ⁶⁷ W. Li, K. Wang, C. Reichhardt, C. J. O. Reichhardt, M. S. Murillo, and Y. Feng, "Depinning dynamics of two-dimensional dusty plasmas on a one-dimensional periodic substrate," *Phys. Rev. E* **100**, 033207 (2019).
- ⁶⁸ L. Gu, W. Li, C. Reichhardt, C. J. O. Reichhardt, M. S. Murillo, and Yan Feng, "Continuous and discontinuous transitions in the depinning of two-dimensional dusty plasmas on a one-dimensional periodic substrate," *Phys. Rev. E* **102**, 063203 (2020).
- ⁶⁹ Y. Huang, W. Li, C. Reichhardt, C. J. O. Reichhardt, and Y. Feng, "Phonon spectra of a two-dimensional solid dusty plasma modified by two-dimensional periodic substrates," *Phys. Rev. E* **105**, 015202 (2022).
- ⁷⁰ W. Zhu, C. Reichhardt, C. J. O. Reichhardt, and Y. Feng, "Directional locking in a two-dimensional Yukawa solid modulated by a two-dimensional periodic substrate," *Phys. Rev. E* **106**, 015202 (2022).
- ⁷¹ K. Pandey, D. Prabhakaran, and S. Basu, "Review of transport processes and particle self-assembly in acoustically levitated nanofluid droplets," *Phys. Fluids* **31**, 112102 (2019).
- ⁷² H. Löwen, "Inertial effects of self-propelled particles: from active Brownian to active Langevin motion," *J. Chem. Phys.* **152**, 040901 (2020).
- ⁷³ M. X. Lim, A. Souslov, V. Vitelli, and H. M. Jaeger, "Cluster formation by acoustic forces and active fluctuations in levitated granular matter," *Nature Phys.* **15**, 460 (2019).
- ⁷⁴ A. Bylinskii, D. Gangloff, I. Counts, and V. Vuletić, "Observation of Aubry-type transition in finite atom chains via friction," *Nature Mater.* **15**, 717–721 (2016).
- ⁷⁵ Y. He, B. Ai, C. Dai, C. Song, R. Wang, W. Sun, F. Liu, and Y. Feng, "Experimental demonstration of a dusty plasma ratchet rectification and its reversal," *Phys. Rev. Lett.* **124**, 075001 (2020).
- ⁷⁶ A. Chugh and R. Ganesh, "Emergence of directed motion in a 2D system of Yukawa particles on 1D ratchet," *Physica A* **593**, 126913 (2022).
- ⁷⁷ Y. Feng, B. Liu, and J. Goree, "Rapid heating and cooling in two-dimensional Yukawa systems," *Phys. Rev. E* **78**, 026415 (2008).
- ⁷⁸ W. F. van Gunsteren and H. J. C. Berendsen, "Algorithms for Brownian dynamics," *Mol. Phys.* **45**, 637–647 (1982).
- ⁷⁹ P. Hartmann, G. J. Kalman, Z. Donkó, and K. Kutasi, "Equilibrium properties and phase diagram of two-dimensional Yukawa systems," *Phys. Rev. E* **72**, 026409 (2005).
- ⁸⁰ G. J. Kalman, P. Hartmann, Z. Donkó, and M. Rosenberg, "Two-dimensional Yukawa liquids: Correlation and dynamics," *Phys. Rev. Lett.* **92**, 065001 (2004).
- ⁸¹ Y. Feng, J. Goree, and B. Liu, "Solid superheating observed in two-dimensional strongly coupled dusty plasma," *Phys. Rev. Lett.* **100**, 205007 (2008).
- ⁸² Y. Feng, J. Goree, and B. Liu, "Longitudinal viscosity of two-dimensional Yukawa liquids," *Phys. Rev. E* **87**, 013106 (2013).
- ⁸³ Y. Feng, J. Goree, B. Liu, L. Wang, and W. Tian, "Pressure of two-dimensional Yukawa liquids," *J. Phys. D: Appl. Phys.* **49**, 235203 (2016).
- ⁸⁴ Y. Feng, W. Lin, and M. S. Murillo, "Viscosity of two-dimensional strongly coupled dusty plasma modified by a perpendicular magnetic field," *Phys. Rev. E* **96**, 053208 (2017).
- ⁸⁵ C. Reichhardt, D. Ray, and C. J. Olson Reichhardt, "Magnus-induced ratchet effects for skyrmions interacting with asymmetric substrates," *New J. Phys.* **17**, 073034 (2015).
- ⁸⁶ W. Chen, L. Liu, and Y. Zheng, "Ultrafast ratchet dynamics of skyrmions by defect engineering in materials with poor conductivity under gigahertz magnetic fields," *Phys. Rev. Applied* **14**, 064014 (2020).
- ⁸⁷ B. Göbel and I. Mertig, "Skyrmion ratchet propagation: utilizing the skyrmion Hall effect in AC racetrack storage devices," *Sci. Rep.* **11**, 3020 (2021).